Enhanced equilibrium distribution functions for simulating immiscible multiphase flows with variable density ratios in...

Article *in* International Journal of Multiphase Flow · December 2013

DOI: 10.1016/j.ijmultiphaseflow.2013.07.001

CITATIONS
17

READS
105

4 authors:

Sébastien Leclaire
Polytechnique Montréal
28 PUBLICATIONS **179** CITATIONS
SEE PROFILE

Nicolas Pellerin
National Research Council
11 PUBLICATIONS **56** CITATIONS
SEE PROFILE

Marcelo Reggio
Polytechnique Montréal
116 PUBLICATIONS **1,142** CITATIONS
SEE PROFILE

Jean-Yves Trépanier
Polytechnique Montréal
176 PUBLICATIONS **1,188** CITATIONS
SEE PROFILE

Enhanced equilibrium distribution functions for simulating immiscible multiphase flows with variable density ratios in a class of lattice Boltzmann models

Sébastien Leclaire*, Nicolas Pellerin, Marcelo Reggio, and Jean-Yves Trépanier

Department of Mechanical Engineering, École Polytechnique,
2500, chemin de Polytechnique, Montreal, Quebec, Canada, H3T 1J4

Abstract

This research examines the behavior of a class of lattice Boltzmann (LB) models designed to simulate immiscible multiphase flows. There is some debate in the scientific literature as to whether or not the "color gradient" models, also known as the Rothman-Keller (RK) models, are able to simulate flow with density variation. In this paper, we show that it is possible, by modifying the original equilibrium distribution functions, to capture the discontinuity present in the analytical momentum profile of the two-layered Couette flow with variable density ratios. Investigations carried out earlier were not able to simulate such a flow correctly. Now, with the proposed approach, the new scheme is compatible with the analytical solution, and it is also possible to simulate the two-layered Couette flow with simultaneous density ratios of $O(1000)$ and viscosity ratios of $O(100)$. To test the model in a more complex flow situation, i.e. with non-zero surface tension and a curved interface, an unsteady simulation of an oscillating bubble with variable density ratio is undertaken. The numerical frequency of the bubble is compared to that of the analytical frequency. It is demonstrated that the proposed modification greatly increases the accuracy of the model compared to the original model, i.e. the error can be up to one order of magnitude lower with the proposed enhanced equilibrium distribution functions. The authors believe that this improvement can be made to other RK models as well, which will allow the range of validity of these models to be extended. This is, in fact, what the authors found for the method proposed in this article.

Keywords: Lattice Boltzmann method, multiphase flow, multicomponent flow, multilayered Couette flow, density ratio, viscosity ratio.

The final publication is available at
http://dx.doi.org/10.1016/j.ijmultiphaseflow.2013.07.001

1. Introduction

Lattice Boltzmann models of multiphase flow can be classified in various categories. One possible classification could be the following :

— the RK from Rothman and Keller [1988] ;
— the SC from Shan and Chen [1993] ;
— the Free-Energy (FE) from Swift et al. [1996] ;
— the Mean-Field (MF) from He et al. [1998] and
— the Field-Mediator (FM) from Santos et al. [2003].

It is worth noting that this classification is not universally adopted, and there are other models, not discussed in this work, that may be classified differently. Our goal here is to improve the RK category, and we begin by providing a short literature review of the RK lattice Boltzmann models.

The RK lattice Boltzmann model for simulating multiphase flow is derived from the lattice gas model of Rothman and Keller [1988]. A couple of years later, Gunstensen et al. [1991] developed a lattice Boltzmann version of the RK model. Grunau et al. [1993] then modified the Gunstensen et al. model to accommodate variable density and viscosity ratios between the fluids in several test cases.

Tölke [2002] and Latva-Kokko and Rothman [2005] realized that the original recoloring step performed at the interface of the fluids in the above model was making the scheme unstable in some situations, or resulting in non physical behavior such as lattice pinning. New recoloring schemes were developed in both studies and the authors of both agreed that the main problem with the original model was a very thin interface between the fluids. Tölke [2002] managed to achieve preliminary simulations that agreed well with experimental data.

Reis and Phillips [2007] changed the forcing scheme of the perturbation operator to induce the appropriate surface tension term in the macroscopic equations. Even without the newest recoloring operators, Reis and Phillips showed that their model could be used to simulate flow with large density ratios in some test cases. Leclaire et al. [2012c] adapted the recoloring operator of Latva-Kokko and Rothman for the Reis and Phillips model in the case of variable density ratios. This modification led researchers to conclude that numerical "noise" in the model could be substantially reduced. Also, higher density ratios were tackled for the same Reis and Phillips test cases. However, as was the case in other studies (Rannou [2008]; Aidun and Clausen [2010]; Yang and Boek [2013]), the current RK model was not able to simulate flow with density variation for the

*. EMAIL : sebastien.leclaire@polymtl.ca

multilayered Poiseuille or Couette flow test cases.

While some sought a cure for this problem, Leclaire et al. [2011] aimed to develop the RK model in order to increase precision in terms of simulating Laplace's law with isotropic discretization for the color gradient. Also, Liu et al. [2012] developed a three-dimensional version of the Reis and Phillips perturbation operator for the D3Q19 lattice. Satisfactory agreement with some experimental results was obtained in the Liu et al. research. Other efforts were also made by Leclaire et al. [2013] to develop an N-phase model. This latter study showed that the RK model was not able to capture the theoretical momentum discontinuity in the simple multilayered Couette flow. Our objective in the current research is to find a solution to this serious problem, which affects RK models in general.

Fortunately, a review of the scientific literature has revealed that models have been developed with demonstrable ability to simulate the multilayered Couette or Poiseuille flow. Lishchuk et al. [2008], for example, developed a multicomponent LB method for fluids with density contrast, which was shown to recover the multilayered Couette flow with a density ratio different from 1. It is not clear, however, how their idea could be used to apply a simple fix to the RK models that were previously not working (Grunau et al. [1993]; Tölke [2002]; Reis and Phillips [2007]; Rannou [2008]; Leclaire et al. [2012c, 2011]; Liu et al. [2012]). Although this basic flow was successfully simulated in the work of Knutson and Noble [2009], the authors clearly state that their method, as presented, is not suitable for more complicated flow configurations, and a great deal of effort is still needed to generalize their method to solving general complex flows. One reason why an attempt is being made to incorporate the level-set method into the lattice Boltzmann method is that the level-set method is better at preserving the volume of the various phases than the lattice Boltzmann method. A volume preserving approach for the multiphase lattice Boltzmann method was studied in the work of Reis and Dellar [2011]. Yiotis et al. [2007] show that their model can simulate the multilayered Poiseuille flow with density ratios ; nevertheless, considerable effort would be required to adapt their ideas to the current RK formulation, as their model use a new pressure distribution function. Recently, a new approach to resolving the discontinuity problem of the RK model, using source terms, has been published by Huang et al. [2013]. This approach is interesting, but different from the one that we are proposing.

Holdych et al. [1998] modified the equilibrium stress tensor of the free energy model of Swift et al. [1996], in order to recover the analytical solution of the multilayered Couette flow with variable density ratios. In fact, we show here that their approach can be readily and easily adapted to the RK model to correctly recover the Navier-Stokes equations in the single phase region with a weak pressure gradient and within the limits of small Mach and Knudsen numbers. Moreover, our method does allow the current RK model to correctly simulate the multilayered Couette flow, even in the case of simultaneous high density $O(1000)$ and high viscosity $O(100)$ ratios. Also, the proposed enhanced equilibrium distribution greatly increases the accuracy of the model with a variable density ratio in a more complex flow situation. This will be illustrated with an unsteady oscillating bubble with a density ratio of $O(100)$, where the numerical frequency of the bubble is compared to its analytical frequency, and much better results are achieved with the proposed modification.

This simple fix can also be applied in a straightforward manner to the following RK model (Grunau et al. [1993]; Tölke [2002]; Reis and Phillips [2007]; Rannou [2008]; Leclaire et al. [2012c, 2011]; Liu et al. [2012]), and perhaps to other LB models with similar issues (Rannou [2008]).

2. Lattice Boltzmann immiscible multiphase model

The current LB approach follows the two-phase model of Reis and Phillips [2007], along with the improvements presented by Leclaire et al. [2012c, 2011, 2013] for the recoloring operator, the isotropic color gradient, and the model generalization to N-phase flows. For this 2D LB model, there are N sets of distribution functions, one for each fluid, moving on a D2Q9 lattice with the velocity vectors $\vec{c_i}$. With $\theta_i = \frac{\pi}{4}(4-i)$, these velocity vectors are defined as :

$$\vec{c_i} = \begin{cases} (0,0), & i = 1 \\ [\sin(\theta_i), \cos(\theta_i)]\, c, & i = 2,4,6,8 \\ [\sin(\theta_i), \cos(\theta_i)]\, \sqrt{2}c, & i = 3,5,7,9 \end{cases} \quad (1)$$

where $c = \Delta x/\Delta t$, $\Delta y = \Delta x$, Δx is the lattice spacing, and Δt is the time step.

The distribution functions for a fluid of color k (e.g. $k = r$ for red, $k = g$ for green, and $k = b$ for blue) are noted $N_i^k(\vec{x}, t)$, while $N_i(\vec{x}, t) = \sum_k N_i^k(\vec{x}, t)$ is used for the color-blind distribution function. The algorithm uses the following evolution equation :

$$N_i^k(\vec{x} + \vec{c_i}\Delta t, t + \Delta t) = N_i^k(\vec{x}, t) + \Omega_i^k(N_i^k(\vec{x}, t)) \quad (2)$$

where the collision operator Ω_i^k is the result of the combination of three sub operators (similar to Tölke [2002]) :

$$\Omega_i^k = (\Omega_i^k)^{(3)} \left[(\Omega_i^k)^{(1)} + (\Omega_i^k)^{(2)} \right] \quad (3)$$

These original operators are rewritten in such a way that the evolution equation is solved in four steps with operator splitting, as follows :

1. Single phase collision operator :
   $N_i^k(\vec{x}, t_*) = (\Omega_i^k)^{(1)}(N_i^k(\vec{x}, t))$

2. Multiphase collision operator (perturbation) :
   $N_i^k(\vec{x}, t_{**}) = (\Omega_i^k)^{(2)}(N_i^k(\vec{x}, t_*))$

3. Multiphase collision operator (recoloring) :
   $N_i^k(\vec{x}, t_{***}) = (\Omega_i^k)^{(3)}(N_i^k(\vec{x}, t_{**}))$

4. Streaming operator :
   $N_i^k(\vec{x} + \vec{c_i}\Delta t, t + \Delta t) = N_i^k(\vec{x}, t_{***})$

The model presented with the evolution equation (2) suggests the use of one set of distribution functions for each fluid. Leclaire et al. [2013] explains how the number of distribution functions necessary for the simulation of N-phase flows can be reduced. Conceptually, only the distribution functions of the color-blind fluid and each density field are required to implement the model, although it is much easier to describe the theoretical model using one set of distribution functions for each fluid.

2.1. Original single phase collision operator

The first sub operator, $(\Omega_i^k)^{(1)}$, is the standard BGK operator of the single phase LB model, where the distribution functions are relaxed towards a local equilibrium, in which ω_{eff} denotes the effective relaxation factor :

$$(\Omega_i^k)^{(1)}(N_i^k) = N_i^k - \omega_{\text{eff}}\left(N_i^k - N_i^{k(e)}\right) \tag{4}$$

Below are the details of this operator. The density of the fluid k is given by the first moment of the distribution functions :

$$\rho_k = \sum_i N_i^k = \sum_i N_i^{k(e)} \tag{5}$$

where the superscript (e) denotes equilibrium. The total fluid density is given by $\rho = \sum_k \rho_k$, while the total momentum is defined as the second moment of the distribution functions :

$$\rho\vec{u} = \sum_i \sum_k N_i^k \vec{c_i} = \sum_i \sum_k N_i^{k(e)} \vec{c_i} \tag{6}$$

in which $\vec{u}$ is the velocity of the color-blind distribution functions. The equilibrium functions are defined by :

$$N_i^{k(e)}(\rho_k, \vec{u}, \alpha_k) = \\ \rho_k\left(\phi_i^k + W_i\left[\frac{3}{c^2}\vec{c_i}\cdot\vec{u} + \frac{9}{2c^4}(\vec{c_i}\cdot\vec{u})^2 - \frac{3}{2c^2}(\vec{u})^2\right]\right) + \Phi_i^k \tag{7}$$

It should be noted that $\Phi_i^k \equiv 0$ for the original single phase collision operator. The weights W_i are those of a standard D2Q9 lattice :

$$W_i = \begin{cases} 4/9, & i = 1 \\ 1/9, & i = 2,4,6,8 \\ 1/36, & i = 3,5,7,9 \end{cases} \tag{8}$$

Besides,

$$\phi_i^k = \begin{cases} \alpha_k, & i = 1 \\ (1-\alpha_k)/5, & i = 2,4,6,8 \\ (1-\alpha_k)/20, & i = 3,5,7,9 \end{cases} \tag{9}$$

As established by Grunau et al. [1993], the various density ratios between fluids k and l are γ_{kl} for two-phase flows, and must be taken as follows to obtain a stable interface :

$$\gamma_{kl} = \frac{\rho_k^0}{\rho_l^0} = \frac{1-\alpha_l}{1-\alpha_k} \tag{10}$$

where the superscript "0" over ρ_k^0 indicates the initial value of ρ_k at the beginning of the simulation.

The pressure of the fluid of color k is :

$$p_k = \rho_k \frac{3(1-\alpha_k)}{5} c^2 = \rho_k (c_s^k)^2 \tag{11}$$

In the above expressions, one of the α_k is a free parameter. We let κ be the index of the least dense fluid. Generally, we set the value of $\alpha_\kappa > 0$, so that the relation $0 < \alpha_\kappa \leq \alpha_k < 1$ is guaranteed to hold for each fluid k. These parameters set the isothermal sound speed c_s^k in each fluid of color k.

Using the index notation (m, n, o, p) and δ for the Kronecker function, Nourgaliev et al. [2003] note that the equilibrium distribution functions $N_i^{k(e)}$ satisfy the following principles of conservation of mass and momentum, momentum flux tensor, and constitutive physics :

$$\sum_i N_i^{k(e)} = \rho_k \tag{12}$$

$$\sum_i N_i^{k(e)} c_{i,m} = \rho_k u_m \tag{13}$$

$$\sum_i N_i^{k(e)} c_{i,m} c_{i,n} = P_{mn}^k + \rho_k u_m u_n \tag{14}$$

$$\sum_i N_i^{k(e)} c_{i,m} c_{i,n} c_{i,o} = \frac{\rho_k c^2}{3}\left(u_m\delta_{no} + u_n\delta_{mo} + u_o\delta_{mn}\right) \tag{15}$$

with the pressure tensor $P_{mn}^k = \rho_k (c_s^k)^2 \delta_{mn}$.

The effective relaxation parameter ω_{eff} is chosen so that the evolution equation, Eq. (2), respects the macroscopic equations for a single phase flow in the single phase regions. When the viscosities of the fluids are different, an interpolation is applied to define the parameter ω_{eff} at the interface.

Like Leclaire et al. [2013], we define the bar functional as the density weighted q-average. For example, for a variable X_k defined for each fluid k, the density weighted q-average of this variable is defined as :

$$\overline{X}\big|_q = \begin{cases} \left(\sum_k \frac{\rho_k (X_k)^q}{\rho}\right)^{\frac{1}{q}}, & q \neq 0 \\ \left(\prod_k (X_k)^{\rho_k}\right)^{\frac{1}{\rho}}, & q = 0 \end{cases} \tag{16}$$

If ν_k is the kinematic viscosity of the fluid k, then, depending on the q-average, one possible choice for the effective relaxation parameter is :

$$\omega_{\text{eff}} = \frac{2c^2\Delta t}{6\left(\overline{\nu}\big|_q\right) + c^2\Delta t} \tag{17}$$

In this study, we use $q = -1$ to interpolate the viscosity $\overline{\nu}\big|_q$ of the fluid. This interpolation corresponds to the density weighted harmonic average. For the simulation of multiphase flows of different viscosities, the interpolation of the viscosity at the interface is a widely used approximation.

In the numerical results section, we show that, with this current form, our model as it stands is not able to correctly simulate

flows with variable density ratios in the two-layered Couette flow. In order to be able to do this, correction terms can be added to the equilibrium distribution functions.

2.2. *Single phase collision operator with enhanced equilibrium*

In their free energy LB model, Holdych et al. [1998] noticed that they were able, by changing the equilibrium distribution functions, to obtain error terms in the macroscopic formulation of the lattice Boltzmann equation compatible with the Navier-Stokes equations under the hypothesis of a weak pressure gradient and within the limits of small Mach and Knudsen numbers. The enhanced equilibrium distribution functions were not given in the original scientific paper of Holdych et al. [1998]. However, Che Sidik and Takahiko [2007] explicitly describe the changes that need to be made to the equilibrium distribution functions in the case of a one-component fluid with a variable density ratio and a "non ideal" equation of state. Their idea is adapted here for our immiscible multiphase RK model, which is aimed at correcting the discontinuity problem in the Couette flow. This approach has not been tested before, and is introduced specifically for the model in this paper. We define Φ_i^k in Eq. (7) such that :

$$\Phi_i^k = \begin{cases} -3\ \overline{\nu}|_q \left(\vec{u}\cdot\vec{\nabla}\rho_k\right)/c, & i=1 \\ +4\ \overline{\nu}|_q \left(\mathbf{G}_k : \vec{c}_i\otimes\vec{c}_i\right)/c^3, & i=2,4,6,8 \\ +1\ \overline{\nu}|_q \left(\mathbf{G}_k : \vec{c}_i\otimes\vec{c}_i\right)/c^3, & i=3,5,7,9 \end{cases} \tag{18}$$

where $\otimes$ is the tensor product and the symbol ":" stand for the tensor contraction. The tensor $\mathbf{G}_k$ is defined by :

$$\mathbf{G}_k = 1/8\left[\left(\vec{u}\otimes\vec{\nabla}\rho_k\right) + \left(\vec{u}\otimes\vec{\nabla}\rho_k\right)^T\right] \tag{19}$$

After summing the equilibrium distribution functions of each fluid k, the color-blind distribution functions $N_i^{(e)}$ are the same as $N_i^{k(e)}$, except that ρ_k is replaced by ρ, and α_k is replaced by $\overline{\alpha}|_{q=1}$. This means that

$$N_i^{(e)} \equiv N_i^{(e)}(\rho,\vec{u},\overline{\alpha}|_{q=1}) = \sum_k N_i^{k(e)}(\rho_k,\vec{u},\alpha_k) \tag{20}$$

With the modifications from Eq. (18), the color-blind distribution functions respect the following constraints of mass and momentum conservation, momentum flux tensor, and constitutive physics :

$$\sum_i N_i^{(e)} = \rho \tag{21}$$

$$\sum_i N_i^{(e)} c_{i,m} = \rho u_m \tag{22}$$

$$\sum_i N_i^{(e)} c_{i,m}c_{i,n} = +P_{mn} + \rho u_m u_n + \overline{\nu}|_q \left[u_m\partial_n(\rho) + u_n\partial_m(\rho) + u_o\partial_o(\rho)\delta_{mn}\right] \tag{23}$$

$$\sum_i N_i^{(e)} c_{i,m}c_{i,n}c_{i,o} = \frac{\rho c^2}{3}\left(u_m\delta_{no} + u_n\delta_{mo} + u_o\delta_{mn}\right) \tag{24}$$

With regard to the color-blind distribution functions, the only difference between the original model ($\Phi_i^k = 0$) and the new model ($\Phi_i^k \neq 0$) is in the definition of the momentum flux tensor, where the terms on the second line of Eq. (23) with a density gradient are added to take into account the density variation in multiphase flow. This is the main idea of Holdych et al. [1998], and is applied here to solve the discontinuity problem of the RK model.

When $\alpha_k = 4/9$, we can see that the color-blind distribution functions of Eq. (20) are the same as those in the free energy model of Che Sidik and Takahiko [2007] in the single phase region. This is because Eqs. (21) to (24) are the same in the single phase region as in the work of Che Sidik and Takahiko [2007]. The only difference is in the pressure tensor P_{mn}, of which we only consider the "ideal" part in our study, so that a different isothermal equation of state is used in each phase :

$$P_{mn} = \rho\frac{3}{5}\left(1-\overline{\alpha}|_{q=1}\right)c^2\delta_{mn} = \rho\ \overline{c_s^2}\Big|_{q=1}\delta_{mn}. \tag{25}$$

Without source terms and in the single phase region only, it is therefore correct to conclude that the color-blind distribution functions of this new model will lead to the same macroscopic equations as defined by Holdych et al. [1998] and Che Sidik and Takahiko [2007] :

$$\partial_t\rho_k + \partial_m(\rho_k u_m) = O(Kn^2) \tag{26}$$

$$\partial_t(\rho_k u_m) + \partial_n(\rho_k u_m u_n) = \tag{27}$$

$$-\partial_n P_{mn}^k + \nu_k\left[\partial_n\rho_k(\partial_n(u_m) + \partial_m(u_n) + \partial_o(u_o)\delta_{mn})\right] \tag{28}$$

$$-3\nu_k\partial_n\left[u_m\partial_o P_{no}^k + u_n\partial_o P_{mo}^k + \partial_o(\rho_k u_m u_n u_o)\right]/c^2 \tag{29}$$

$$-3\nu_k\partial_n\left[(\partial_n P_{mn}^k)(\partial_o\rho_k u_o)\right]/c^2 \tag{30}$$

$$-3\nu_k\partial_n\left[u_m\partial_o(u_n\partial_o\rho_k + u_o\partial_n\rho_k + \delta_{on}u_p\partial_p\rho_k)\right]/c^2 \tag{31}$$

$$-3\nu_k\partial_n\left[u_n\partial_o(u_m\partial_o\rho_k + u_o\partial_m\rho_k + \delta_{mo}u_p\partial_p\rho_k)\right]/c^2 \tag{32}$$

$$+3\nu_k\partial_n\left[\partial_t(u_m\partial_n\rho_k + u_n\partial_m\rho_k + \delta_{mn}u_p\partial_p\rho_k)\right]/c^2 + O(Kn^2) \tag{33}$$

where the first three lines are the compressible continuity and Navier-Stokes momentum equations, and the subsequent lines are the error terms, all negligible with weak pressure gradients and within the small Mach and Knudsen Kn number limit (Holdych et al. [1998]). In fact, if ν_k is of order one, the analysis performed by Holdych et al. [1998] assumes that the pressure gradient should be at most $O(\vec{u})$.

Again, the single phase collision operator is chosen to respect the macroscopic equations of a single phase flow in the single phase region only. Most multiphase LB models do not consider the viscosity variation in the theoretical development of the model (Grunau et al. [1993]; Dupin et al. [2003]; Kang et al. [2004]; Halliday et al. [2009]). As in this model, the development is achieved by first supposing a constant viscosity, and then applying an interpolation to describe the viscosity at the interface. It is important to note that the interpolation of the viscosity at the interface is a method commonly used in other multiphase flow models (Lafaurie et al. [1994]; Akhlaghi Amiri and Hamouda [2013]). The viscosity interpolation is

already used in the definition of the relaxation factor ω_{eff}, and here we only apply the viscosity interpolation $\overline{\nu}|_q$ once more to construct the correction terms Φ_i^k. In fact, it is not clear what happens at the interface because of this interpolation. However, based on the numerical results, it seems that our method effectively corrects the discontinuity problem of the RK model in the two-layered Couette flow.

2.3. Perturbation operator

Surface tension in the RK model is modeled by means of the perturbation operator (Halliday et al. [1998]; Reis and Phillips [2007]; Gunstensen et al. [1991]). To introduce surface tension into this model, a "color" gradient $\vec{F}_{kl}$ would need to be defined first, which approximates the normal interfaces for each of the k-l fluid interfaces. With multiple interfaces, a simplification is made such that the surface tension between each pair of fluids is taken into account, but the interaction related to surface tension between two fluids in an interface does not depend on the presence of the other fluids. In others words, as in Dupin et al. [2003], the two-phase flow theory is applied individually to each k-l fluid interface.

The color gradient in this model is defined as :

$$\vec{F}_{kl} = \frac{\rho_l}{\rho}\vec{\nabla}\left(\frac{\rho_k}{\rho}\right) - \frac{\rho_k}{\rho}\vec{\nabla}\left(\frac{\rho_l}{\rho}\right) \tag{34}$$

For flow with three phases or more, this formulation for the color gradient has been shown to be superior to the usual RK color gradient (Leclaire et al. [2013]).

The perturbation operator for the fluid k is therefore defined by

$$(\Omega_i^k)^{(2)}(N_i^k) = N_i^k + \sum_{\substack{l \\ l\neq k}} \frac{A_{kl}}{2}|\vec{F}_{kl}|\left[W_i\frac{(\vec{F}_{kl}\cdot\vec{c}_i)^2}{|\vec{F}_{kl}|^2c^2} - B_i\right] \tag{35}$$

with

$$B_i = \begin{cases} -4/27, & i = 1 \\ 2/27, & i = 2,4,6,8 \\ 5/108, & i = 3,5,7,9 \end{cases} \tag{36}$$

Note that this scheme does not require a concentration factor, as in the model of Dupin et al. [2003]. A careful interpretation of the color gradient in Eq. (34) can reveal that a concentration is not needed with this definition. This is one advantage of the formulation given by Eq. (34).

Reis and Phillips [2007] has shown that the perturbation operator complies, within the macroscopic limit, with the capillary stress tensor present in the macroscopic equations for two-phase flows. It handles the coupling between the two fluids, with the space- and time-dependent parameters A_{kl} chosen to model the surface tension at the k-l fluid interface.

The surface tension σ_{kl} is set as follows :

$$\sigma_{kl} = \frac{1}{9}\frac{(A_{kl}+A_{lk})}{\omega_{\text{eff}}}c^2\Delta t \tag{37}$$

The values for σ_{kl} are set at the beginning of a simulation. However, the values for $A_{kl} = A_{lk}$ are space- and time-dependent, because ω_{eff} may depend on space and time.

Although this operator generates the surface tension, it does not guarantee the fluid's immiscibility. To minimize the mixing and segregate the fluids, the recoloring operator $(\Omega_i^k)^{(3)}$ needs to be properly selected.

2.4. Recoloring operator

This latter operator is used to maximize the amount of fluid of color k at the interface that is sent to the k fluid region, while respecting the conservation of mass and total momentum. The recoloring operator presented here is a combination of the essential ideas in Latva-Kokko and Rothman [2005] and Halliday et al. [2007], and is as follows :

$$(\Omega_i^k)^{(3)}(N_i^k) = \frac{\rho_k}{\rho}N_i + \sum_{\substack{l \\ l\neq k}} \beta_{kl}\frac{\rho_k\rho_l}{\rho^2}\cos(\varphi_i^{kl})N_i^{(e)}(\rho, 0, \overline{\alpha}|_{q=1}) \tag{38}$$

where β_{kl} is a parameter controlling the thickness of the k-l interface. The variable φ_i^{kl} corresponds to the angle between the color gradient $\vec{F}_{kl}$ and the lattice direction vector $\vec{c}_i$. The equilibrium distributions of the color-blind fluid $N_i^{(e)}$ in Eq. (38) are evaluated using Eq. (7), a zero velocity, and the respective value of $\overline{\alpha}|_{q=1}$. This operator keeps the fluids immiscible while conserving the mass and momentum of the color-blind fluid and the mass of each individual fluid k. The momentum dynamics of each fluid k is not conserved, or, more accurately, does not exist, in this model. However, it should be noted that, in each single-phase region, the color-blind fluid coincides with each fluid of color k. So, it is only at the interface that some information concerning the individual momentum dynamics of each fluid k is lost.

2.5. Isotropic discrete gradient operator

Generally, a fourth order isotropic discrete gradient operator is used for the discretization of the gradient in Eqs. (18) and (34). This kind of isotropic gradient operator was presented by Sbragaglia et al. [2007] for 2D and 3D, and further generalized by Leclaire et al. [2012b] for higher order spatial and isotropic operators. Leclaire et al. [2011] show that this type of discretization enhances the accuracy of the RK model significantly. The fourth order isotropic gradient operator takes the following form :

$$\vec{\nabla}f(x,y) = \left[\frac{\partial}{\partial x}, \frac{\partial}{\partial y}\right]f(x,y) \approx \sum_{i=1}^{9}\frac{\xi_i\left[d_i^x, d_i^y\right]f(x+d_i^x, y+d_i^y)}{(\Delta x)^2} \tag{39}$$

with

$$\begin{aligned} \vec{\xi} &= [0,4,1,4,1,4,1,4,1]/12 \\ \vec{d}^x &= [0,0,1,1,1,0,-1,-1,-1]\Delta x \\ \vec{d}^y &= [0,1,1,0,-1,-1,-1,0,1]\Delta x \end{aligned} \tag{40}$$

Note that this operator supposes that $\Delta y = \Delta x$. To compute this type of gradient efficiently, convolution products may be used, as explained by Leclaire et al. [2012a,b]. In this study, a 4^{th} order isotropic gradient is used for the simulation of the two-layered Couette flow, while an 8^{th} order isotropic gradient is used for the simulation of the unsteady oscillating bubble (Leclaire et al. [2013]).

2.6. Adjustment of the interface width for static contact angles

For three-phase flows, and when the surface tension yields a Neumann triangle, there is a possible equilibrium state where static contact angles θ_{kl} will be formed between the fluids. Spencer et al. [2010] found, and demonstrated theoretically, that a particular relation for β_{kl} at the triple fluid junction must be used, otherwise the angle θ_{kl} will not be satisfied at steady state. The value of the angle θ_{kl} can be found from the surface tension σ_{kl} using the law of cosines. By setting $\theta_{\max}$ as the largest θ_{kl}, the special relations for β_{kl} are as follows :

$$\beta_{kl} = \begin{cases} \beta^0, & kl \text{ with } \theta_{\max} \\ \beta^0 \left(1 + c_{triple} \left(\sin(\pi - \theta_{\max} - \theta_{kl}) - 1\right)\right), & \text{otherwise} \end{cases} \tag{41}$$

where β^0 is a constant between 0 and 1 controlling the overall thickness of all three interfaces, and

$$c_{triple} = \min\left\{\eta_2 \frac{\rho_r \rho_g \rho_b}{\rho^3}, 1\right\} \tag{42}$$

is a function that also varies between 0 and 1. The free threshold $\eta_2 = 35$. This value for η_2 has been shown to provide good results (Leclaire et al. [2013]). However, in this study, these special relations are not used, and each β_{kl} is set to the same constant.

3. Numerical Simulation

3.1. Two-layered Couette flow

The purpose of this numerical test is to investigate the model's ability to simulate flow with variable dynamic viscosity. The two-layered Couette flow consists of two layers of fluid between two infinite moving plates.

The variable x_I is used to denote the interface position between the fluids with properties (ρ_r, μ_r) on the left-hand side and (ρ_b, μ_b) on the right-hand side, where $\mu_k = \rho_k \nu_k$ is the dynamic viscosity. The walls located at positions x_0 and x_N move vertically at a velocity of u_0^y and u_N^y respectively.

At steady state and applying the incompressibility hypothesis, an analytical solution exists for the previous flow setting (Leclaire et al. [2013]). This leads to two theoretical momentum profiles within each interval $x_0 \leq x < x_I$ and $x_I < x \leq x_N$ of the form :

$$(\rho u^y)(x)|_{\text{th}} = \begin{cases} \rho_r^0(a_r x + b_r), & x_0 \leq x < x_I \\ \rho_b^0(a_b x + b_b), & x_I < x \leq x_N \end{cases} \tag{43}$$

with the constants a_r, b_r, and a_b, and b_b solutions of the following system :

$$\begin{pmatrix} x_0 & 1 & 0 & 0 \\ \mu_r & 0 & -\mu_b & 0 \\ x_I & 1 & -x_I & -1 \\ 0 & 0 & x_N & 1 \end{pmatrix} \cdot \begin{pmatrix} a_r \\ b_r \\ a_b \\ b_b \end{pmatrix} = \begin{pmatrix} u_0^y \\ 0 \\ 0 \\ u_N^y \end{pmatrix} \tag{44}$$

Now that the analytical solution for the two-layered Couette flow has been presented, the setting for this test is described in the context of an LB simulation. It is common in lattice Boltzmann methods to set the lattice spacing $\Delta x = 1$ and the time step Δt so that $c = 1$. We do this here. Since the analytical solution is one-dimensional, a lattice containing $N_x = 160$ by $N_y = 1$ sites is used, unless stated otherwise, and is located over the interval $[x_0, x_N]$. The interface $x_I = (x_0 + x_N)/2$ is located halfway along the channel, and each fluid section is initialized with the zero velocity equilibrium distribution functions. The wall located at x_0 and x_N passes over the lattice sites, while the interfaces x_I pass between the fluid lattice sites. Because the model is 2D, periodic boundary conditions are applied in the y-direction. The first and last sites are located where the velocity boundary conditions are implemented. The standard Zou and He [1997] velocity boundary condition is applied. The wall velocities are set to $u_0^y = 0.0001$ and $u_N^y = -0.01$. The values $\alpha_\kappa = 4/9$ (κ index of the least dense fluid) and $\beta_{kl} = 0.8$ are used. The density $\rho_b = 1$, and the viscosity $\nu_r = 1/2$.

A special nomenclature, shown in Table (1), is introduced to describe the various simulations. Depending on the simulation case, with its different density and viscosity ratios, additional information is provided in Table (2).

Nomenclature	
U	Unit
L	Low
M	Medium
H	High
D	Density ratio
V	Viscosity ratio

Table 1: Nomenclature used for the various simulation cases.

Case	ρ_r/ρ_b	ν_r/ν_b	# Table
UD-LV	1	2	(3)
UD-MV	1	20	(3)
UD-HV	1	100	(3)
LD-UV	2	1	(4)
MD-UV	20	1	(4)
HD-UV	1000	1	(4)
LD-LV	2	2	(5)
MD-MV	20	20	(5)
HD-HV	1000	100	(5)

Table 2: Additional simulation parameters for the two-layered Couette flow.

As previously explained by Leclaire et al. [2013], the initial condition for this problem can lead to instability, because the color-blind density distribution N_1 and the fluid densities ρ_k are initially discontinuous. In this case, it is preferable to initialize the flow with a more continuous function. To do so, the model equations are solved for a certain number of time steps with $A_{kl} = 0$, while $\vec{u} = 0$ is imposed in the equilibrium density distribution in Eq. (7). So, for the simulations presented here, the first 2000 time steps only serve to stabilize the initial density distribution and fluid densities to a more continuous function.

Note that the numerical steady state is regarded as achieved when :

$$\max_{\text{all sites}} \left\{ \left| \frac{(N_i)^{(n)} - (N_i)^{(n-1)}}{(N_i)^{(n)}} \right| \right\} \leq \epsilon \tag{45}$$

with $\epsilon = 10^{-10}$, while n denotes the time step number. To reduce the computational cost, this condition is only checked every 2000 time steps.

3.1.1. Discussion of the numerical results

To compare the original model ($\Phi_i^k = 0$) and the new model ($\Phi_i^k \neq 0$) in terms of the numerical and theoretical momentum profiles, three sets of simulations were undertaken. The first set, shown in Table (3), contains simulations that illustrate the behavior of the two models with unit density but variable viscosity ratios. The second set, given in Table (4), illustrates the case with variable density ratios, but a unit viscosity ratio. The last set, shown in Table (5), presents the case with both variable density and variable viscosity ratios. All the tables, (3) to (5), display cases with unit and/or low, medium, and high density and/or viscosity ratios. The numerical density profiles are not shown, because both models are able to capture the theoretical density profile correctly in all cases.

The results in Table (3) indicate that the behavior of the momentum in the original model is identical to that in the new model, with unit density and variable viscosity ratios. This is because $\Phi_i^k = 0$ when the density gradient is zero. In fact, without density variation, the two models become theoretically the same. The work of Leclaire et al. [2012c] shows that the model is able to simulate the multilayered Poiseuille flow with a very high viscosity ratio $O(10000)$, but with unit density ratio only. Therefore, it is not surprising that this model is also able to simulate the two-layered Couette flow with unit density ratio and large viscosity ratios.

With variable density and unit viscosity ratios, the results in Table (4) reveal that the behavior of the momentum in the original and in the new model are different. In fact, in our case here, the original model yields a momentum profile which is not affected at all by the change in density across the interface. This clearly indicates the inability of the original model to simulate flows with variable density ratios. In contrast, the new model shows the expected theoretical behavior, i.e. the discontinuity in the momentum profile is well captured by the numerical scheme.

With both variable density and variable viscosity ratios, the results displayed in Table (5) indicate that the behavior of the momentum in the original and in the new model are again different. Only the new model works as expected. Even when using viscosity interpolation, the new model is still able to capture the two-layered Couette flow correctly. Our tests indicate that the scheme is stable, with a simultaneous density ratio of $O(1000)$ and a viscosity ratio of $O(100)$. Any further increase in viscosity ratio leads to instability.

For each of the nine tests, Table (6) shows the L2 errors that occur with the new model as the lattice size increases. It is clear that the proposed model is compatible with the analytical solution, as the order of accuracy is > 1. It is important to point out that the model is only second order accurate in space with unit density ratios for this test case. With variable density ratios, a discontinuity arises in the momentum profile and the order of accuracy drops to 1. We can see that the `MD-MV` case yielded an order of accuracy of 1.478, but this is only because the jump discontinuity is small for this situation, and the momentum profile decreases monotonically.

Overall, the approach presented in this paper enhances the range of validity of this RK model. Moreover, there is every reason to expect that this technique will also work for the other RK models (Grunau et al. [1993]; Tölke [2002]; Reis and Phillips [2007]; Rannou [2008]; Leclaire et al. [2012c, 2011]; Liu et al. [2012]), which also suffer from the discontinuity problem. The current approach should correct the behavior of these models with respect to momentum for the test case involving the multilayered Couette flows with variable density ratios.

3.2. Unsteady oscillating bubble

This last numerical simulation experiment, consisting of an unsteady oscillating bubble, is provided to check the behavior of the proposed scheme in a more complex flow situation. In effect, an oscillating bubble simulation is in an unsteady regime with a curved interface and non-zero surface tension. Also, a density ratio exists between the two phases. The goal of the test is to compare the numerical frequency of the bubble with that of the analytical one.

The setting of this test for a lattice Boltzmann simulation is as follows. We used $\Delta x = \Delta y = \Delta t = c = 1$, as with the Couette flow simulations. A lattice size of $N_x = 128$ and $N_y = 128$ sites is used, located over the computational domain $[1, 128] \times [1, 128]$. The red and blue fluids are initialized with zero velocity equilibrium distribution functions. The sites corresponding to the red fluid are within the following initial ellipse :

$$\frac{(x - 64.5)^2}{16^2} + \frac{(y - 64.5)^2}{24^2} < 1 \tag{46}$$

The blue fluid occupies the other sites. Some of the simulation parameters are given by : $\rho_r = 1$, $\rho_b = 1/100$, and $\nu_r = \nu_b = 1/30$. The values $\alpha_\kappa = 4/9$ (κ index of the least dense fluid) and $\beta_{kl} = 1$ are used. As described with the two-layered Couette flow simulations, the initial condition may lead to instability, so again, the first 2000 time steps only serve to stabilize the initial density distribution and fluid densities to a more continuous function.

As described by Toutant [2006] and Lemonnier and Jamet [2004], theoretically, if the fluid is inviscid and two-dimensional, the angular frequency ω_n for each mode of the oscillations is :

$$\omega_n^2 = \frac{n(n+1)(n-1)}{\rho_r + \rho_b} \frac{\sigma_{rb}}{R^3} \tag{47}$$

and the associated oscillating period T_n is given by :

$$T_n = \frac{2\pi}{\omega_n} \tag{48}$$

Note that n is the mode number and R is the equivalent radius of the bubble at equilibrium. As stated by Toutant [2006], we are only interested in the second mode ($n = 2$), because it corresponds to an ellipsoidal initial shape, as in our lattice Boltzmann setting. It is important to realize that, even if the lattice Boltzmann scheme does not neglect the viscous effect, these are sufficiently small in the current numerical experiment to illustrate that the proposed enhanced equilibrium distribution function behaves better than the original one.

To extract the numerical data from the simulations in order to compare the results with the analytical value, we first define $\psi = (\rho_r - \rho_b)/(\rho_r + \rho_b)$, the corresponding color field. The shape of the bubble at a given time is then given by the contour $\psi = 0$. The analytical frequency, ω_{the}, is computed using Eq. (47) and with the radius R approximate at a given time t with $R = \sqrt{(A_{\psi=0}/\pi)}$, where $A_{\psi=0}$ is the area enclosed by the contour $\psi = 0$ at time t. The numerical frequency of the bubble, ω_{num}, is extracted from Eq. (48). To approximate the period of the oscillations, we proceed as follows : First, a cubic spline is computed from ψ at the sites given at $x = 64$ and $64.4 < y < 128$. Given this spline, we compute the zero of this function as time passes in the simulation. This provides a function $y_{\psi=0}(t)$. There is another cubic spline that can be used to interpolate this function over time, from which we can extract the local maxima and minima by computing the time derivative of the spline. To avoid some initial noise in the data, we start recording the various maxima and minima after only 500 time steps. Then we extract $t^{(1)}$, $t^{(2)}$, $t^{(3)}$, and $t^{(4)}$ corresponding to the time at which a maximum or a minimum occurs. The period $T_{n=2}$ is approximate, with $2(t^{(4)} - t^{(3)})$. Finally, the simulations are stopped at time $t = t^{(4)}$.

3.2.1. *Discussion of the numerical results*

In total, six simulations are undertaken to study the behavior of the new model versus that of the original model. The oscillation frequencies of the original and the new model are compared in Table (7) for different surface tensions σ_{rb}. Also, to illustrate the bubble oscillation, Fig. (1) shows, for example with the new model, the contour of the bubble when $\sigma_{rb} = 0.005$. The snapshot of the contour corresponds to the time at which a maximum or a minimum of the function $y_{\psi=0}(t)$ occurs.

The only difference between the original model ($\Phi_i^k = 0$) and the new model ($\Phi_i^k \neq 0$) is the term Φ_i^k. All the supplementary errors related to the original model compared to those related to the new model can be associated with the fact that Φ_i^k is missing in the original model. For the various tests performed, the error can be up to one order of magnitude lower with the proposed enhanced equilibrium distribution functions. It is clear that the proposed modification is useful for complex flow simulation with a variable density ratio. Note that any further significant increase in the density ratio would render the scheme unstable. So, in the unsteady regime, the range of applicability of the model is limited by the density ratio.

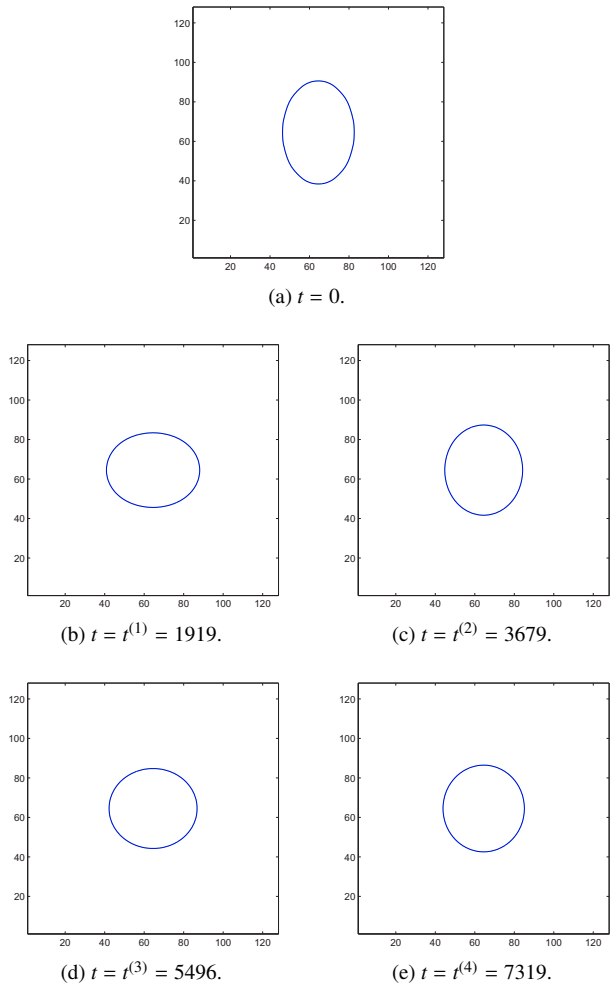

(a) $t = 0$.

(b) $t = t^{(1)} = 1919$.

(c) $t = t^{(2)} = 3679$.

(d) $t = t^{(3)} = 5496$.

(e) $t = t^{(4)} = 7319$.

FIGURE 1: Bubble contour in an unsteady simulation with the new model, $\sigma_{rb} = 0.005$ and a density ratio of $O(100)$.

4. Conclusion

In this research, the equilibrium distribution functions of the current RK lattice Boltzmann model have been modified to correctly recover the Navier-Stokes equations with weak pressure gradients and within the limits of a small Mach and Knudsen number. Because of the way in which the original model was used by various researchers, it was not able to capture the momentum discontinuity in the two-layered Couette flow with density ratios other than 1. The new model is able to do so, even with a large density ratio $O(1000)$ and a viscosity ratio $O(100)$. Also, an unsteady bubble simulation with a variable

density ratio of $O(100)$ has shown that the analytical frequency of the bubble is better captured with the proposed enhanced equilibrium distribution functions. However, the discontinuity problem of the RK models mentioned by Aidun and Clausen [2010] is only partially resolved, since the model is valid only when the pressure gradients are weak, which is usually the case when the current isothermal equation of state is used. We also believe that other LB models in the RK class, and perhaps even other classes, could also use the current corrected equilibrium distribution functions to improve their range of validity. We end this article on this final note : It is important to acknowledge that most of the test cases examined in our previous works (Leclaire et al. [2011, 2012c, 2013]) are still valid with the current corrected equilibrium. This is because the original model and the new model coincide within the limit of 0 momentum or of 0 density gradient. Often in these works, one of the two conditions is, for practical purposes, met.

Acknowledgments

The authors thank the anonymous reviewers for their insightful and constructive comments. We applied the SDC (sequence-determines-credit) approach in listing the authors of this article (Tscharntke et al. [2007]). The work was supported by a grant from the NSERC (Natural Sciences and Engineering Research Council of Canada).

Références

Aidun, C. K., Clausen, J. R., 2010. Lattice-boltzmann method for complex flows. Annual Review of Fluid Mechanics 42 (1), 439–472.

Akhlaghi Amiri, H. A., Hamouda, A. A., 2013. Evaluation of level set and phase field methods in modeling two phase flow with viscosity contrast through dual-permeability porous medium. International Journal of Multiphase Flow 52 (0), 22–34.

Che Sidik, N. A., Takahiko, T., 2007. Two-phase flow simulation with lattice boltzmann method. Jurnal Mekanikal 24, 68–79.

Dupin, M. M., Halliday, I., Care, C. M., 2003. Multi-component lattice boltzmann equation for mesoscale blood flow. Journal of Physics A : Mathematical and General 36 (31), 8517–8534.

Grunau, D., Chen, S., Eggert, K., 1993. A lattice boltzmann model for multiphase fluid flows. Physics of Fluids A : Fluid Dynamics 5 (10), 2557–2562.

Gunstensen, A. K., Rothman, D. H., Zaleski, S., Zanetti, G., 1991. Lattice boltzmann model of immiscible fluids. Physical Review A 43, 4320–4327.

Halliday, I., Hollis, A. P., Care, C. M., 2007. Lattice boltzmann algorithm for continuum multicomponent flow. Physical Review E 76 (2), 026708.

Halliday, I., Spencer, T. J., Care, C. M., 2009. Validation of multicomponent lattice boltzmann equation simulations using theoretical calculations of immiscible drop shape. Physical Review E 79 (1), 016706.

Halliday, I., Thompson, S. P., Care, C. M., 1998. Macroscopic surface tension in a lattice bhatnagar-gross-krook modelof two immiscible fluids. Physical Review E 57, 514–523.

He, X., Shan, X., Doolen, G. D., 1998. Discrete boltzmann equation model for nonideal gases. Physical Review E 57 (1), R13–R16.

Holdych, D. J., Rovas, D., Georgiadis, J. G., Buckius, R. O., 1998. An improved hydrodynamics formulation for multiphase flow lattice-boltzmann models. International Journal of Modern Physics C 09 (08), 1393–1404.

Huang, H., Huang, J.-J., Lu, X.-Y., Sukop, M. C., 2013. On simulations of high-density ratio flows using color-gradient multiphase lattice boltzmann models. International Journal of Modern Physics C 24 (04), 1350021.

Kang, Q., Zhang, D., Chen, S., 2004. Immiscible displacement in a channel : simulations of fingering in two dimensions. Advances in Water Resources 27 (1), 13–22.

Knutson, C., E., Noble, D., R., 2009. Embedding sharp interfaces within the lattice boltzmann method for fluids with arbitrary density ratios. Eur. Phys. J. Special Topics 171, 21–29.

Lafaurie, B., Nardone, C., Scardovelli, R., Zaleski, S., Zanetti, G., 1994. Modelling merging and fragmentation in multiphase flows with surfer. Journal of Computational Physics 113 (1), 134–147.

Latva-Kokko, M., Rothman, D. H., 2005. Diffusion properties of gradient-based lattice boltzmann models of immiscible fluids. Physical Review E 71, 056702.

Leclaire, S., El-Hachem, M., Reggio, M., 2012a. MATLAB - A Fundamental Tool for Scientific Computing and Engineering Applications - Volume 3. InTech, Ch. Convolution Kernel for Fast CPU/GPU Computation of 2D/3D Isotropic Gradients on a Square/Cubic Lattice, pp. 195–216.

Leclaire, S., El-Hachem, M., Trépanier, J.-Y., Reggio, M., 2012b. High order spatial generalization of 2d and 3d isotropic discrete gradient operators with fast evaluation on gpus, submitted results.

Leclaire, S., Reggio, M., Trépanier, J.-Y., 2011. Isotropic color gradient for simulating very high-density ratios with a two-phase flow lattice boltzmann model. Computers & Fluids 48 (1), 98–112.

Leclaire, S., Reggio, M., Trépanier, J.-Y., 2012c. Numerical evaluation of two recoloring operators for an immiscible two-phase flow lattice boltzmann model. Applied Mathematical Modelling 36 (5), 2237–2252.

Leclaire, S., Reggio, M., Trépanier, J.-Y., 2013. Progress and investigation on lattice boltzmann modeling of multiple immiscible fluids or components with variable density and viscosity ratios. Journal of Computational Physics (0), –.

Lemonnier, H., Jamet, D., 2004. Test-cases for interface tracking methods. Ch. Test-case number 5 : Oscillation of an inclusion immersed in a quiescent fluid (PA), pp. 41–47.

Lishchuk, S. V., Halliday, I., Care, C. M., 2008. Multicomponent lattice boltzmann method for fluids with a density contrast. Physical Review E 77 (3), 036702.

Liu, H., Valocchi, A. J., Kang, Q., 2012. Three-dimensional lattice boltzmann model for immiscible two-phase flow simulations. Physical Review E 85 (4), 046309.

Nourgaliev, R. R., Dinh, T. N., Theofanous, T. G., Joseph, D., 2003. The lattice boltzmann equation method : theoretical interpretation, numerics and implications. International Journal of Multiphase Flow 29 (1), 117–169.

Rannou, G., 2008. Lattice-boltzmann method and immiscible two-phase flow. Master's thesis.

Reis, T., Dellar, P., 2011. A volume-preserving sharpening approach for the propagation of sharp phase boundaries in multiphase lattice boltzmann simulations. Computers & Fluids 46 (1), 417 – 421.

Reis, T., Phillips, T. N., 2007. Lattice boltzmann model for simulating immiscible two-phase flows. Journal of Physics A : Mathematical and Theoretical 40 (14), 4033–4053.

Rothman, D. H., Keller, J. M., 1988. Immiscible cellular-automaton fluids. Journal of Statistical Physics 52 (3), 1119–1127.

Santos, L. O. E., Facin, P. C., Philippi, P. C., 2003. Lattice-boltzmann model based on field mediators for immiscible fluids. Physical Review E 68 (5), 056302.

Sbragaglia, M., Benzi, R., Biferale, L., Succi, S., Sugiyama, K., Toschi, F., 2007. Generalized lattice boltzmann method with multirange pseudopotential. Physical Review E 75 (2), 026702.

Shan, X., Chen, H., 1993. Lattice boltzmann model for simulating flows with multiple phases and components. Physical Review E 47, 1815–1820.

Spencer, T. J., Halliday, I., Care, C. M., 2010. Lattice boltzmann equation method for multiple immiscible continuum fluids. Physical Review E 82 (6), 066701.

Swift, M., Orlandini, E., Osborn, W., Yeomans, J., 1996. Lattice boltzmann simulations of liquid-gas and binary fluid systems. Physical Review E 54, 5041–5052.

Tölke, J., 2002. Lattice boltzmann simulations of binary fluid flow through porous media. Philosophical Transactions of the Royal Society of London. Series A : Mathematical, Physical and Engineering Sciences 360 (1792), 535–545.

Toutant, A., 2006. Modelisation physique des interactions entre interfaces et turbulence. Ph.D. thesis, Institut National Polytechnique de Toulouse.

Tscharntke, T., Hochberg, M. E., Rand, T. A., Resh, V. H., Krauss, J., 2007. Author sequence and credit for contributions in multiauthored publications. PLoS Biol 5 (1), e18.

Yang, J., Boek, E. S., 2013. A comparison study of multi-component lattice boltzmann models for flow in porous media applications. Computers & Mathematics with Applications (0).

Yiotis, A. G., Psihogios, J., Kainourgiakis, M. E., Papaioannou, A., Stubos, A. K., 2007. A lattice boltzmann study of viscous coupling effects in immiscible two-phase flow in porous media. Colloids and Surfaces A : Physicochemical and Engineering Aspects 300 (1-2), 35–49.

Zou, Q., He, X., 1997. On pressure and velocity boundary conditions for the lattice boltzmann bgk model. Physics of Fluids 9 (6), 1591–1598.

TABLE 3: Two-layered Couette flow with *unit* density and *variable* viscosity ratios.

Case	Momentum : ρu^y	
	Original model	New model
UD-LV	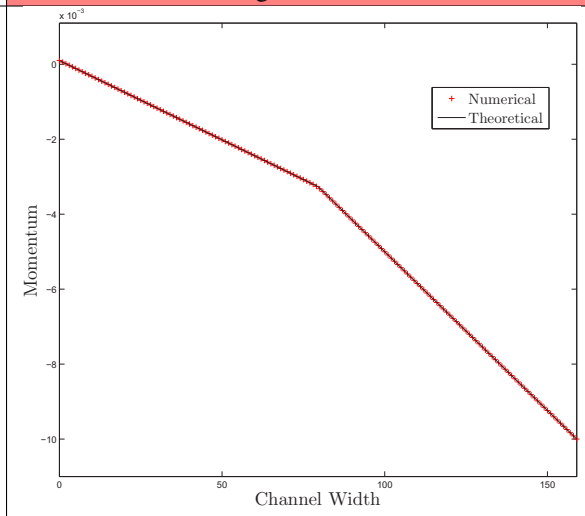	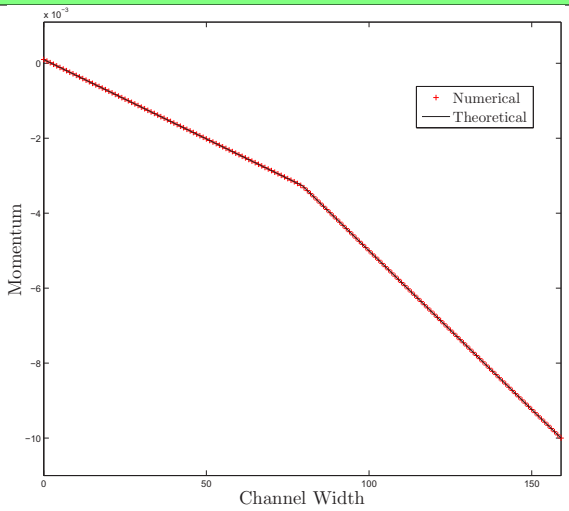
UD-MV	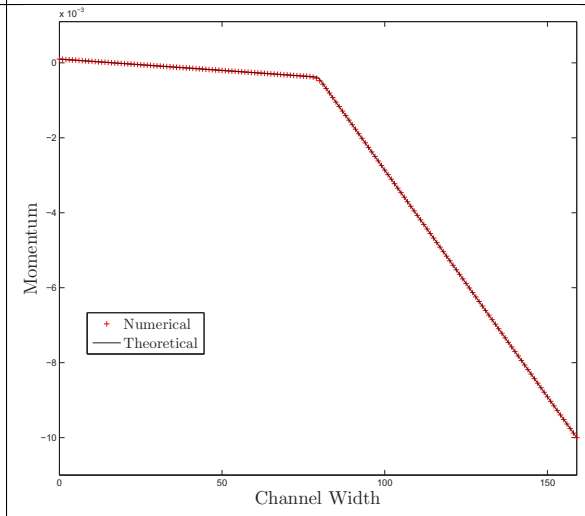	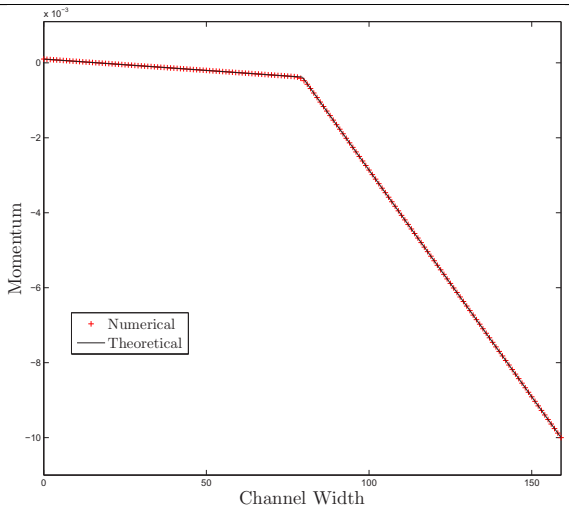
UD-HV	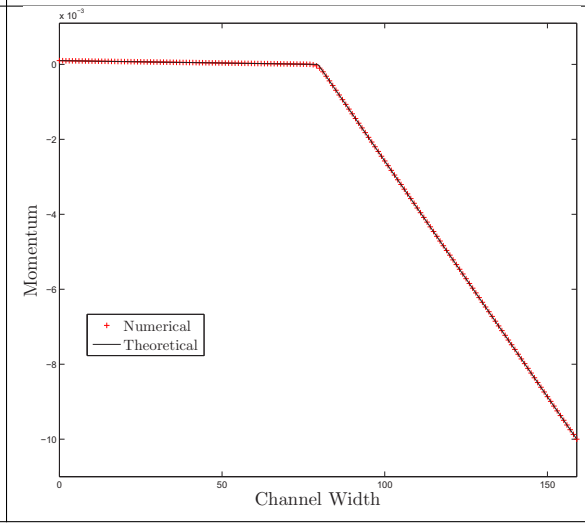	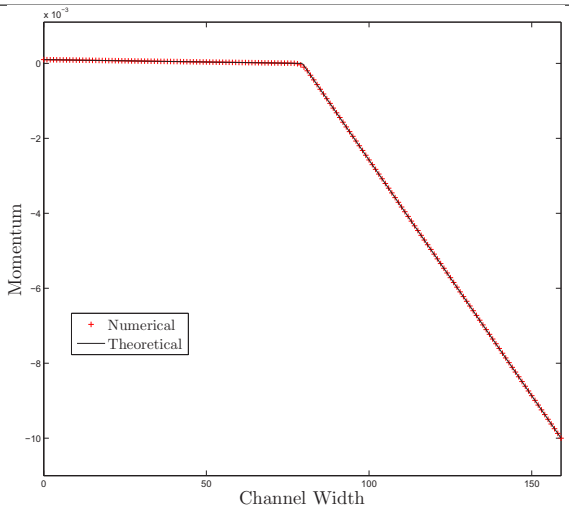

TABLE 4: Two-layered Couette flow with *variable* density and *unit* viscosity ratios.

Case	Momentum : ρu^y	
	Original model	New model
LD-UV	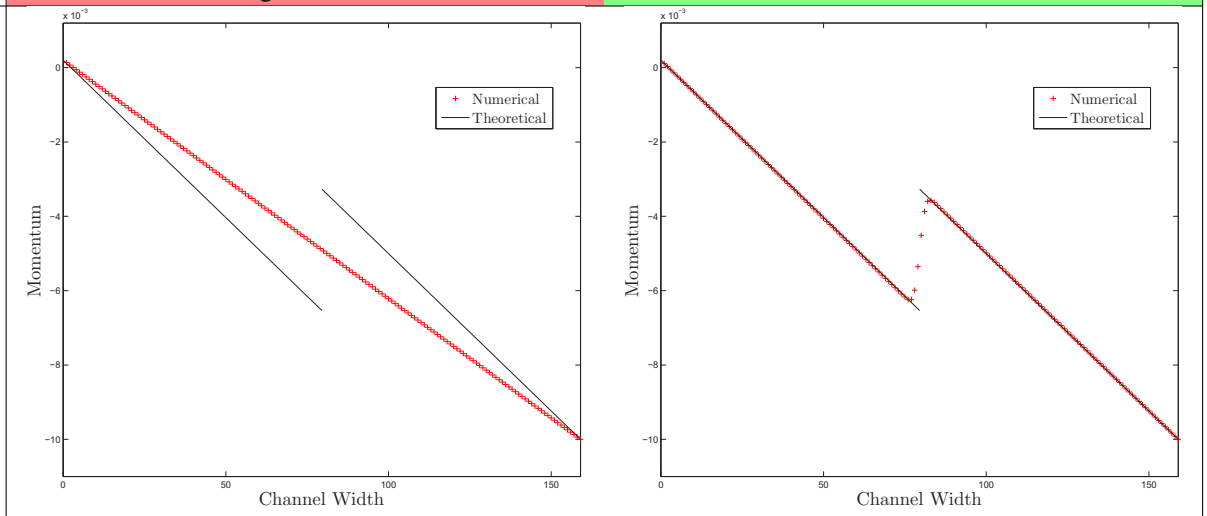	
MD-UV	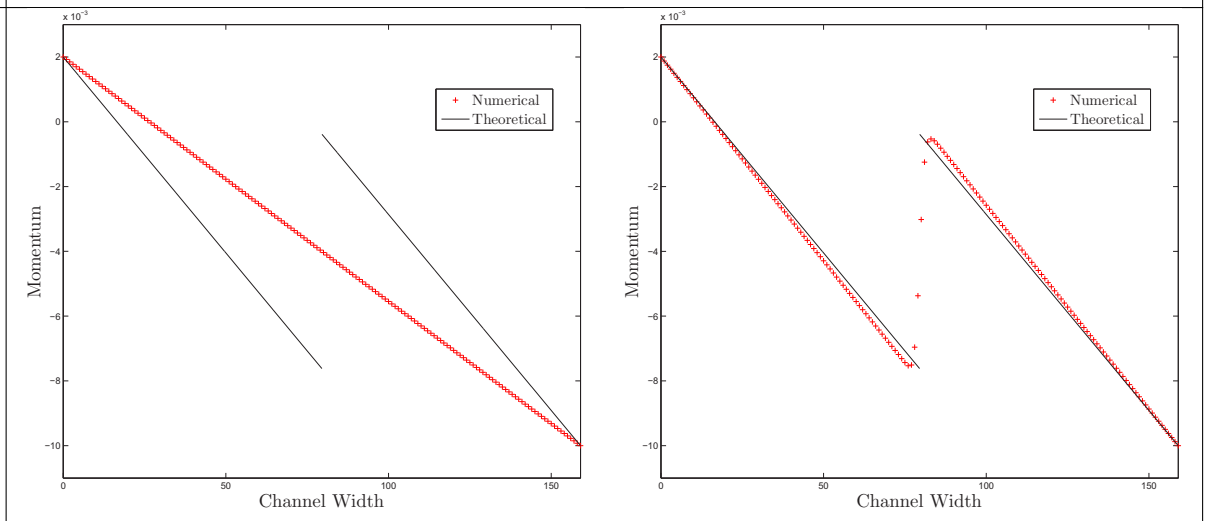	
HD-UV	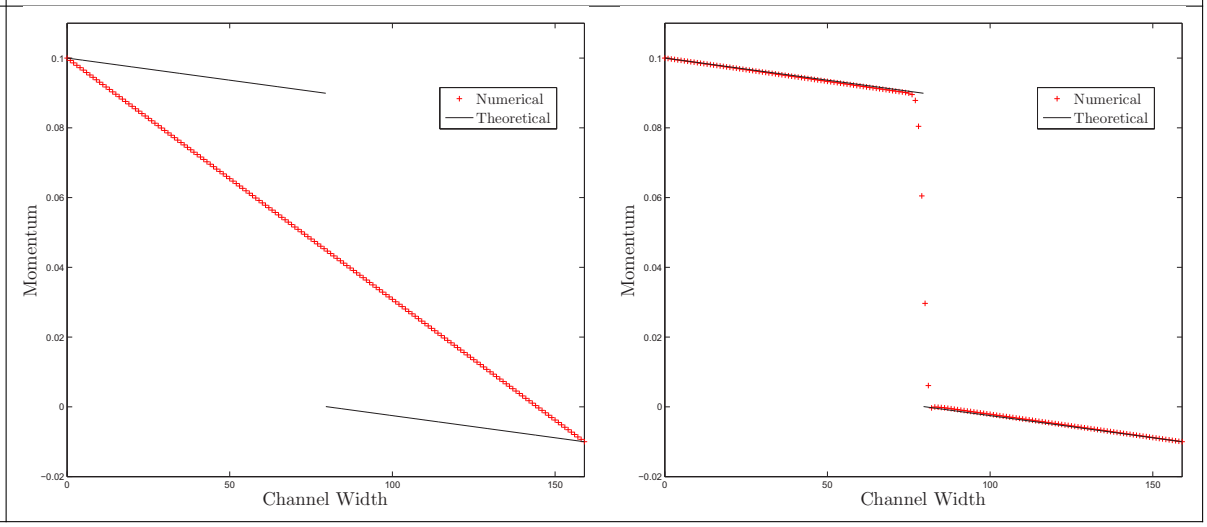	

TABLE 5: Two-layered Couette flow with *variable* density and *variable* viscosity ratios.

Case	Momentum : ρu^y	
	Original model	New model
LD-LV	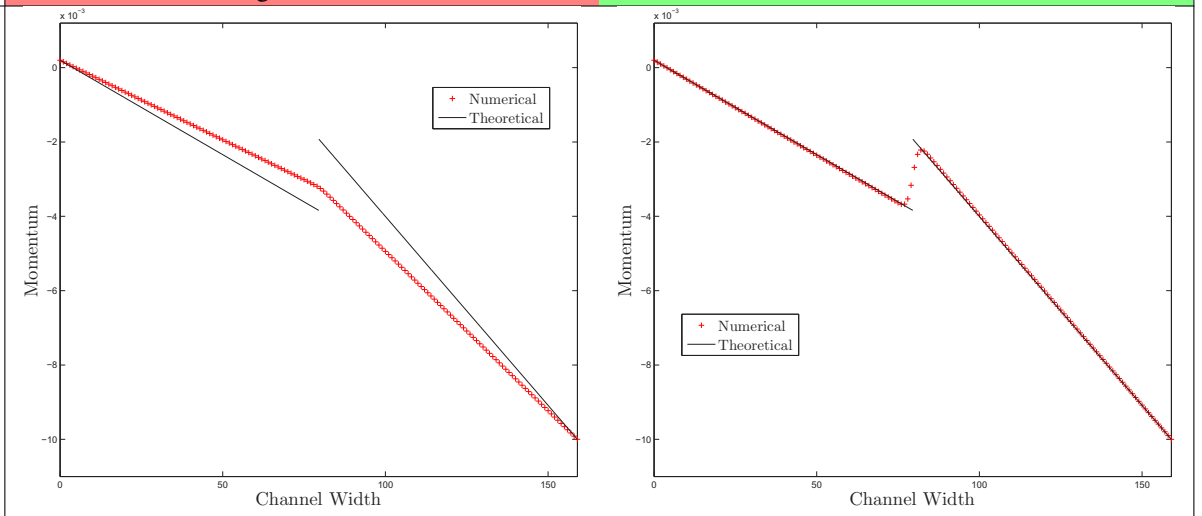	
MD-MV	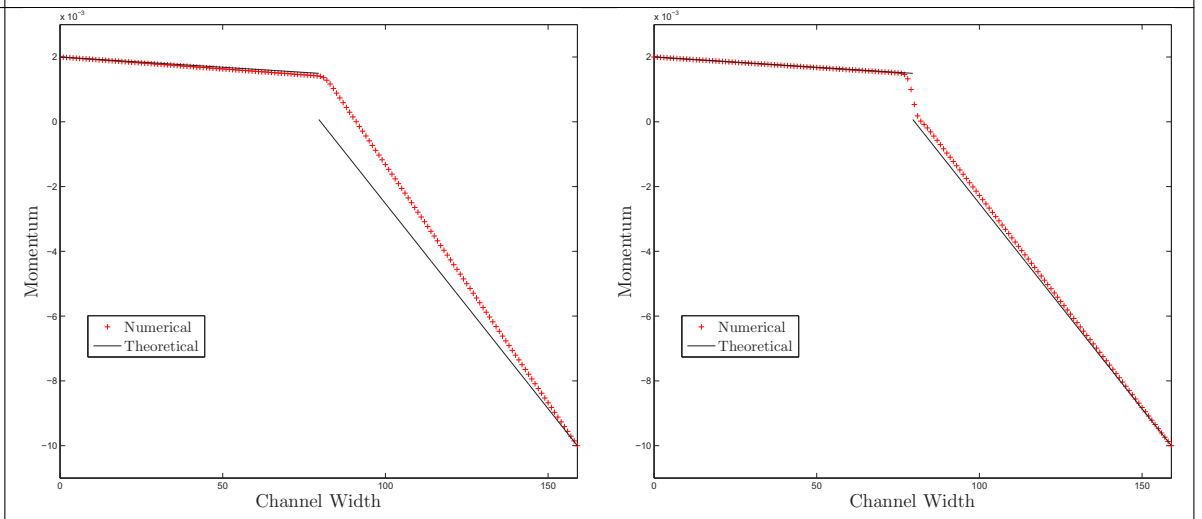	
HD-HV	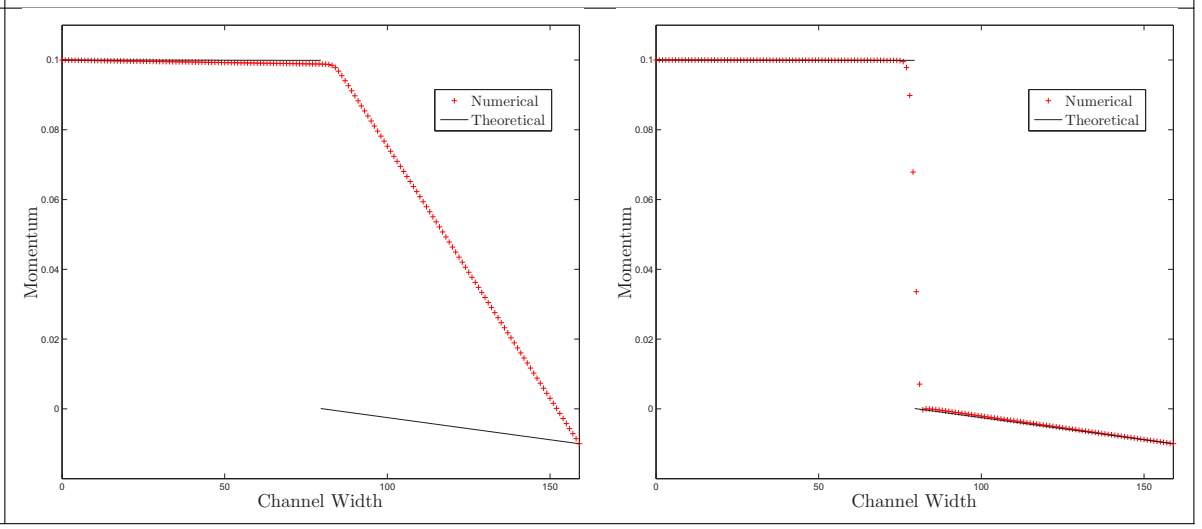	

$\sqrt{\frac{\sum_j \left((\rho u^y)(x_j)\big\|_{\text{th}} - (\rho u^y)(x_j)\big\|_{\text{num}} \right)^2}{N_x - 1}}$				
Case	$N_x = 40$	$N_x = 80$	$N_x = 160$	Order
UD-LV	1.004e-04	2.468e-05	6.175e-06	2.012
UD-MV	1.389e-03	3.500e-04	8.802e-05	1.990
UD-HV	2.372e-03	5.903e-04	1.485e-04	1.999
LD-UV	1.160e-03	4.035e-04	1.417e-04	1.517
MD-UV	3.264e-03	1.032e-03	3.461e-04	1.619
HD-UV	2.967e-02	9.998e-03	3.457e-03	1.551
LD-LV	7.097e-04	2.426e-04	8.635e-05	1.519
MD-MV	3.884e-03	1.125e-03	3.564e-04	1.723
HD-HV	3.729e-02	1.308e-02	4.758e-03	1.485

TABLE 6: Errors between theoretical and numerical momentum for the two-layered Couette flow and the new model.

		ω_{num}		Error (%)	
σ_{rb}	ω_{the}	Original model	New model	Original model	New model
$5 \cdot 10^{-3}$	1.759E-03	1.637E-03	1.723E-03	6.94	2.04
$1 \cdot 10^{-3}$	7.615E-04	6.646E-04	7.554E-04	12.0	0.81
$5 \cdot 10^{-4}$	5.364E-04	4.223E-04	5.065E-04	21.3	5.58

TABLE 7: Error between the theoretical and numerical frequency of various oscillating bubbles.